1812

LA-4624

MASTER

LOS ALAMOS SCIENTIFIC LABORATORY
of the
University of California
LOS ALAMOS • NEW MEXICO

Bremsstrahlung Emission Measurement from Thick Tungsten Targets in the Energy Range 12 to 300 kV

UNITED STATES
ATOMIC ENERGY COMMISSION
CONTRACT W-7405-ENG. 36

Printed in the United States of America. Available from
National Technical Information Service
U. S. Department of Commerce
5285 Port Royal Road
Springfield, Virginia 22151
Price: Printed Copy $3.00; Microfiche $0.95

Written: November 1970
Distributed: April 1971

LA-4624
UC-34, PHYSICS
TID-4500

LOS ALAMOS SCIENTIFIC LABORATORY
of the
University of California
LOS ALAMOS • NEW MEXICO

Bremsstrahlung Emission Measurement from Thick Tungsten Targets in the Energy Range 12 to 300 kV

by

Ellery Storm
Harvey I. Israel
Douglas W. Lier

BREMSSTRAHLUNG EMISSION MEASUREMENT FROM THICK TUNGSTEN TARGETS IN THE ENERGY RANGE 12 TO 300 kV

by

Ellery Storm
Harvey I. Israel
Douglas W. Lier

ABSTRACT

X-ray spectral measurements were made using four commercial, tungsten-target, x-ray units operating between 12 and 300 kV. The absolute intensity as well as the spectral distribution was measured. The effect of varying the tube current, target aperture, and detector aperture was investigated. The intensity from two constant-potential units was proportional to the tube current, but two self-rectified units displayed a departure from linearity as the tube current increased. As the target aperture area was increased, the photon intensity increased rapidly at first, but then leveled off to a constant value. The intensity was found to vary directly with the area of the detector aperture, but the spectra became distorted when the aperture was increased to where the counting rate exceeded 1.2×10^4 counts/sec. Sodium iodide scintillators, germanium, and silicon semiconductors, and a xenon proportional counter were used to measure the spectra. The measurements were corrected for Gaussian broadening, efficiency, escape peak losses, Compton scattering, and energy linearity to obtain an estimate of the undistorted spectra incident on the detectors. The estimate was used as the input to a computer program that simulated the detectors. The estimate was revised until the calculation gave satisfactory agreement with the spectral measurements of all four detector types. The best estimates of the spectra incident on the detector were corrected for the attenuation of the intervening air, Mylar windows, detector windows, and inherent filtration. After correcting for the solid angle subtended by the detector, the absolute intensity and spectral distribution emitted from the target was obtained for each x-ray unit operating between its minimum and maximum potentials. The total photon and energy fluxes in the L lines, K lines, and continuum are given, as well as the jump ratio at the K edge. The x-ray production efficiency was found to increase from 0.025% at 12 kV to 1% at 300 kV. The constant of proportionality varied in the range $(0.22 \text{ to } 0.74) \times 10^{-6}$ $(\text{kV})^{-1}$

I. INTRODUCTION

This paper presents the results of an experimental study of thick-target bremsstrahlung emission from four commercial x-ray units, operating between 12 and 300 kV. Absolute photon intensities as well as spectral intensity distributions are given. Previous spectral measurements in this

energy region[1-14] have been summarized elsewhere.[15-18] In most cases, the results are given in terms of relative photon intensities and the measurements have been made with scintillation spectrometers, although germanium detector measurements have been reported.[19] In recent experimental thick-target bremsstrahlung studies,[20,21] the observation angle as well as the target material has been varied.

The measurements described in this paper were made with four detector types: a silicon semiconductor, a germanium semiconductor, a xenon proportional counter, and a sodium iodide scintillator. After correcting for Gaussian broadening, escape peak losses, efficiency, Compton scattering, and energy linearity, an estimate of the "true" or undistorted spectrum was made. A computer program employing Monte Carlo techniques was used to calculate the measured spectrum to be expected for a given geometry and resolution when a narrow, parallel beam of photons was normally incident on a detector. The estimate of the undistorted spectrum was revised until the Monte Carlo calculation gave satisfactory agreement with the spectral measurements obtained with all four detector types. The final estimate of the undistorted spectrum is given, together with the average measurements obtained with all four detectors and the Monte Carlo calculation of the measured spectrum for each detector. The final undistorted spectrum was corrected back to the target, and values were obtained for the absolute intensity and spectral distribution.

The x-ray units, the detectors, and the experimental arrangement and procedure are described in Sec. II. The results obtained may vary with changes in experimental parameters such as tube current, target aperture, and detector aperture. These variations are discussed in Sec. III. The measurements are presented in Sec. IV along with a discussion of the results.

II. EXPERIMENTAL DETAILS

a. X-Ray Units

Four x-ray units were studied: a 300-kV Norelco, a 275-kV Triplett-Barton, a 100-kV Picker, and a 60-kV Picker.

The constant-potential Norelco MG-300 industrial x-ray unit contains an oil-immersed Müller MÖ 301/10 tube. The tungsten target is at an angle of 22.5° from the central ray and projects a 5-mm-square focal spot. The exciting potential can be varied from 100 to 300 kV, and the tube current ranges from 2 to 10 mA. This tube has a relatively large amount of inherent filtration. This may be seen from the sketch of the tube (Fig. 1), which includes the location of the filament, target, and inherent filtration. This tube had been in operation more than 3000 h, and it appeared possible that some of the tungsten had boiled off the target and was deposited on the beryllium window, adding to the inherent filtration. To determine if this had occurred, a similar tube with 3700 h of operation was obtained from the manufacturer and disassembled. An examination of the beryllium window disclosed less than 10^{-5} g/cm^2 of tungsten on the window.

The self-rectified Triplett-Barton Tri-Ind-X portable radiographic unit has a resonant transformer and tube head, containing a Machlett EG-252-C beryllium window tube with a water-cooled, grounded anode and gas (SF_6) insulation. The tungsten target is at an angle of 20° from the central ray and projects a 4.5-mm-square focal spot. The maximum voltage is said to be 275 kV; however, it was found that dial settings of 35, 58, 79, 150, 223, and 275 kV corresponded to exciting potentials of 60, 80, 100, 150, 200, and 235 kV, respectively. The tube current can be varied between 1 and 10 mA.

The self-rectified Picker diagnostic x-ray unit contains a Machlett MR-100 Pyrex glass tube, which is air insulated and cooled. It operates between 40 and 100 kV at currents between 1 and 20 mA. The tungsten

TABLE I

DESCRIPTION OF X-RAY UNITS

X-Ray Unit	X-Ray Tube[a]	Voltage Range (kV)	Current Range (mA)	Wave Form	Target Area (cm^2)	Target Angle (°)	Inherent Filtration (g/cm^2)
North American Philips Co. (Norelco)	Müller MÖ 301/10	100 - 300	2 - 10	Constant-potential	0.25	22.5	0.65 Pyrex glass 0.71 Araldit plastic 0.44 beryllium 1.4 oil
Triplett & Barton, Inc.	Machlett EG-252-C	60 - 200	1 - 10	Self-rectified	0.20	20	0.425 beryllium
Picker X-Ray Corp.	Machlett MR-100	40 - 100	1 - 20	Self-rectified	0.10	20	0.28 Pyrex glass
Picker X-Ray Corp.	Machlett OEG-60G	12 - 60	2 - 50	Constant-potential	0.36	45	0.046 beryllium

[a]All four x-ray tubes had tungsten targets.

target is at an angle of 20° with the central ray and projects a 3.2-mm-square focal spot.

The constant-potential Picker diffraction unit contains a Machlett OEG-60G beryllium window tube, which is oil insulated and water-cooled, and has a grounded anode. The exciting potential can be varied from 12 to 60 kV at currents from 2 to 50 mA. The tungsten target is at an angle of 45° with the central ray, and the projected focal spot is a 6-mm square.

The "rayproof" housings of all four x-ray units were found to leak radiation. Consequently, lead, varying in thickness from 0.6 to 2.5 cm, was used to shield the tube housing and cable connectors to ensure that only the exit window emitted radiation. The more important features of the x-ray units are summarized in Table I.

b. Detectors

The spectral measurements were made with five detectors: a germanium semiconductor, a silicon semiconductor, a xenon proportional counter, and two sodium iodide scintillators. A thicker, more efficient sodium iodide detector with an aluminum window was used at the higher potentials, and a thinner sodium iodide detector with a beryllium window at the lower potentials. The dimensions, window thickness, and orientation of each detector are given in Table II. A detailed description of the resolution, Gaussian broadening, photopeak efficiency, escape peak losses, Compton scattering, and linearity of each detector has been reported previously.[22]

c. Arrangement and Procedure

Figure 2 shows the essential features of the experimental arrangement. The cable connectors and x-ray tube, except for the exit window, were completely encased in lead shielding to prevent radiation leakage. Electrically actuated lead and tungsten shutters over the exit windows provided remote beam control. The area of the target aperture was varied by placing 2.5-cm-thick lead blocks having different diameter holes over the exit window.

To reduce the counting rate to a measurable level, the detectors were placed approximately 50 m from the x-ray target. Because air attenuation is appreciable over this distance, an Orangeburg pipe that could be evacuated was placed between the target and the detector. The 15-cm-diam Orangeburg pipe had a cardboard base covered with tar. Each pipe joint was sealed with a Silastic sealant, and the ends of the pipe were closed with a Mylar window 0.0105 g/cm^2 thick. The pipe was evacuated by means of two vacuum pumps attached approximately 10 m from each end of the pipe. Pressures of 1 to 2 mm of Hg were obtained. The air between the x-ray tube window and first Mylar pipe window, the air in the pipe, and the

TABLE II

DESCRIPTION OF DETECTORS

Manufacturer	Model No.	Detector Type	Cylindrical Dimensions Diameter (cm)	Cylindrical Dimensions Length (cm)	Window Thickness (g/cm^2)	Orientation
Harshaw Chemical Co.	12 S12	Sodium Iodide scintillator	7.62	7.62	0.274 Al	Photons incident on plane surface
Harshaw Chemical Co.	8SH B2	Sodium Iodide scintillator	5.08	1.27	0.046 Be	Photons incident on plane surface
Reuter-Stokes Electronic Components, Inc.	RSG 30A	Xenon proportional counter	4.44	10.5	0.046 Be	Photons incident on curved surface
Ortec, Inc.	8047	Germanium (Li-drifted) semiconductor	2.28	0.75	0.046 Be	Photons incident on curved surface
Technical Measurements Corp.	332A	Silicon (Li-drifted) semiconductor	1.27	0.30	0.046 Be	Photons incident on plane surface

air between the second Mylar pipe window and the detector window had a total thickness of 0.035 to 0.055 g/cm^2. The effect of the pipe on the spectral measurements may be seen from Fig. 3, which shows 100- to 300-kV Norelco x-ray spectra obtained without the pipe and with an air-filled pipe, employing a sodium iodide detector. At lower potentials, there is no significant difference between the spectra, but at higher potentials, the measurements with the pipe give slightly but consistently higher intensities which can be explained in terms of small-angle scatter.

Two types of detector apertures were used. First, cylindrical, 2.5-cm-thick lead shields, containing small holes, were placed over the detector. Later, a brass-lead plate with a hole 3.2 cm in diameter was centered over the Mylar window at the end of the pipe. Two bolts attached to the plate supported a 6.4-cm-diam, 2.5-cm-thick lead disk with the hole. The detector, completely shielded except for its window, was placed against the disk. This arrangement was easier to align than the first arrangement and gave identical results.

The shielded detector was placed on a stand that permitted orientation in any desired direction. The detector was aligned by sighting through the detector aperture at a light placed in the target aperture. After optical alignment, spectral measurements were made with small changes in the orientation of the detector to see if the counting rate could be increased. When the detectors were aligned, the intensity varied directly with the detector aperture. Measurements with three different aperture areas were made with each spectrum measurement to ensure that the detectors were aligned and not overloaded. Background was measured with the x-ray unit on and a lead plug in the detector aperture. The background counting rate was less than 0.1% of that of the direct beam, except for the germanium detector which had a high leakage current, resulting in a large background current in the lowest channels.

Pulse-height analysis of all spectra was performed with a Victoreen Scipp 500-channel analyzer, which, along with the amplifiers and output equipment, was housed in a small trailer near the detector. The preamplifiers, amplifiers and method of calibration used with each detector have been described elsewhere.[22] The analyzer gain was set so that one channel width corresponded

to a 1-keV interval. The channel-width-per-keV interval setting was checked daily before and after each run, and only occasionally was it necessary to adjust the fine gain. The measurements were repeated over a period of 4 yr. Only rarely were changes in spectra observed exceeding 20%.

III. PARAMETER VARIATIONS

a. Tube Current

The effects of varying the tube current were investigated with all four x-ray units. The shape of the x-ray spectrum was not significantly affected when the current was varied; however, changes in intensity per mA were observed. The largest effects were observed with the Triplett-Barton unit. Spectral measurements obtained with this unit at 1, 2, 4, 6, 8, and 10 mA at 150 kV are shown in Fig. 4. For ease of comparison, the time was adjusted to give the same mA-min. The intensity per mA decreases nearly linearly as the tube current increases. This may be seen from Fig. 5, where the average ratio of the count obtained at a given energy and current, to the count obtained at the same energy at 1 mA is plotted as a function of tube current for this unit. The ratios were calculated at every 5-keV interval from the data in Fig. 4. The standard deviation shown with each point is indicative of the constancy of the spectral shape as well as of the statistical fluctuations. Similar plots for the other three units are also shown in Fig. 5. The 100-kV Picker unit, which like the Triplett-Barton is self-rectified, shows the same tendency for the intensity per mA to decrease as the current is increased. A calibrated ammeter connected in series with the current meter on the x-ray control panel was used to measure the current. Our final spectral measurements were made at the lowest current in each case.

b. Target Aperture

The effects of varying the target aperture were studied with the Triplett-Barton and Norelco x-ray units. In both cases the projected target size was approximately 5 mm square. The target consists of a rectangular piece of tungsten, 1.6 by 2.1 cm, embedded in a copper anode. The Norelco tube that was disassembled after operating 3700 h was discolored in a 4 by 7 mm rectangle in the center of the tungsten. The target aperture appeared to have a small effect on the spectral shape, but the absolute intensity was quite sensitive to the aperture area. This may be seen from Fig. 6, which shows 200-kV spectra, measured with a germanium detector and a fixed detector aperture (0.00941 cm^2), from the Triplett-Barton unit with various apertures placed over the exit window of the tube. Similar 200-kV spectra were obtained with the Norelco unit using a sodium iodide detector.

To determine if the spectral shape was affected by the target aperture, the count obtained at a given energy with an aperture was divided by the count obtained at the same energy with the largest aperture, and this ratio was plotted as a function of energy for each 5-keV interval. The results are shown in Fig. 7 for two apertures each from the Triplett-Barton and Norelco measurements. Although the statistical fluctuations are large, the ratio tends to decrease as the energy increases. Count ratios, such as those shown in Fig. 7, were averaged for each aperture and are plotted in Fig. 8 as a function of the aperture area. Also indicated in Fig. 8 is the projected target area, 0.25 cm^2. The count ratio increases nearly linearly with a slope of about 4 up to the target area. As the target area is exceeded, the count ratio continues to rise another factor of 2 until an area about 4 times that of the target area is reached, where it levels off and becomes constant. The factor of 2 increase in intensity above the target area indicates, perhaps, that the apertures were not properly aligned. If small target apertures are used to decrease the beam intensity, great care must be taken to ensure that the aperture remains aligned. To avoid this difficulty, in the remainder of our spectral measurements, we used target

aperture areas which in each case exceeded the target area by at least a factor of 6.

c. Detector Aperture

The effects of varying the detector aperture were studied with all four x-ray units and all four detector types. The intensity was found to vary directly with the detector aperture area. However, if the detector aperture area was too large, the higher counting rate overloaded the detector and the measured spectra were distorted. Typical results are given in Fig. 9, which shows the 100-kV Triplett-Barton spectrum measured with various apertures over the germanium detector. For ease of comparison, the counting time was adjusted to give the same cm^2-min. Table III gives the area, the live counting time, and the total counts/sec for each aperture. Figure 9 shows the measured points obtained with the three smallest apertures very close to one another, indicating that the intensity varied directly with the aperture area up to an area of 0.04 cm^2, or a counting rate of 1.2×10^4 counts/sec. When the area was 0.114 cm^2, or the counting rate increased to 9.8×10^4 counts/sec, the intensity decreased at the lower energies and increased at the higher energies. As the area was increased further, more and more counts were lost in the lower energies and were recorded at the higher energies owing to coincidence effects. At an area of 0.635 cm^2, the counting rate, 3×10^6 counts/sec, was so high that all trace of the L- and K-line structure was lost and counts were recorded at energies as high as 200 keV, although the exciting potential was only 100 kV. Thus, even at a detector distance of 50 m from the target, with a large target aperture (2.85 cm^2), at the lowest tube current permitted by the unit (1 mA), the detector aperture area must be relatively small (less than 0.04 cm^2) to prevent the detector from being overloaded and distorting the spectrum. Hypodermic needles were embedded in three detector shields to ensure true holes and determine if the spectral measurements were influenced by the atomic number of the detector aperture. The spectra measured with the hypodermic needle apertures showed no significant differences from those obtained with simple holes in the lead shield.

TABLE III

DETECTOR APERTURES

Area (cm^2)	Counting Time (min)	Total (Counts/sec)
0.00941	33.7	6.7×10^2
0.0201	15.8	3.0×10^3
0.0401	7.9	1.2×10^4
0.114	2.8	9.8×10^4
0.203	1.6	3.0×10^5
0.317	1.0	7.6×10^5
0.635	0.5	3.0×10^6

IV. RESULTS

a. The Measured Bremsstrahlung Spectra

The measured x-ray spectra are presented in Figs. 10 to 29. For each of the four x-ray units there are five figures. The first figure gives our final estimate of the undistorted spectra on the detector. The points in the next four figures give the measurements obtained with the silicon, germanium, sodium iodide, and xenon detectors. The experimental conditions of these measurements are given in Table IV. The solid lines in these four figures give the Monte Carlo calculation's prediction of how each detector would measure the undistorted spectra given in the first figure.

The method of estimating the undistorted spectrum and the details of the Monte Carlo calculation have been reported in a separate paper.[22] Briefly, given the estimate of the undistorted spectrum, the detector geometry, and the detector resolution, the program calculates the spectrum each detector would measure assuming a narrow, parallel beam of incident photons. In general, the Monte Carlo calculations of the silicon, germanium, and sodium iodide detector spectra are in good agreement with the measurements. Because of large leakage currents in the germanium detector, it was necessary to suppress the counting rate in the

TABLE IV

EXPERIMENTAL CONDITIONS FOR FIGS. 10 to 29

X-Ray Unit	Detector Area (cm^2)	Time (sec)	Energy Interval (keV)	Tube Current (mA)	X-Ray Target to Detector Distance (cm)	Intervening Material (g/cm^2)	Inherent Filtration (g/cm^2)
300-kV Norelco	0.00941	510	1	2	4920	0.046 Be 0.021 Mylar 0.052 Air	0.44 Be 1.4 Oil 0.71 Araldit plastic 0.65 Pyrex glass
275-kV Triplett-Barton	0.00941	510	1	1	4797	0.046 Be 0.021 Mylar 0.046 Air	0.425 Be
100-kV Picker	0.00941	510	1	2	4787	0.046 Be 0.021 Mylar 0.036 Air	0.28 Pyrex glass
60-kV Picker	0.0010	480	1	2	4655	0.046 Be 0.021 Mylar 0.037 Air	0.046 Be

lower channels, so that the measured values lie well below the calculations. The largest discrepancies between measurement and calculation are observed with the xenon proportional counter. Each measured spectrum represents the average of 10 to 20 individual measurements. After a review of the uncertainties due to statistical errors, detector corrections, analyzer instabilities, and geometry errors, the accuracy of the experimental spectral intensities given in Figs. 11 to 14, 16 to 19, 21 to 24, and 26 to 29 is estimated to be 10%. After a comparison of the experimental and Monte Carlo calculated spectra, the accuracy of the undistorted spectra given in Figs. 10, 15, 20, and 25 is estimated to be 15% above 15 keV and 25% below 15 keV.

b. Target Spectra

To compare the measurements to theory,[15,23-28] the data must be corrected for the attenuation of the intervening material, which includes air, the Mylar pipe windows, the detector window, and the inherent filtration. The intervening material is given in Table IV, and cross-section tables[29] are available which permit one to correct for the attenuation. In addition, Table IV gives the detector aperture and x-ray target to detector distance so that corrections can be made for the solid angle in steradians subtended by the detector. The counting time, tube current, and energy interval are also listed in Table IV. Thus, the spectra incident on the detector, shown in Figs. 10, 15, 20, and 25, were corrected for the attenuation of the intervening material including the inherent filtration and converted to units of photons/sec-mA-keV-sr to estimate the intensity from the x-ray target. The results are given in Figs. 30 to 33 for the four x-ray units. For purposes of clarity the L and K lines have been omitted.

The 100-kV Picker and the 300-kV Norelco spectra fall off sharply below 10 and 20 keV, respectively, because of their relatively large inherent filtration. Consequently, the intensity below these energies was indeterminable. The inherent filtration of the 60-kV Picker and 275-kV Triplett-Barton units consisted only of beryllium tube windows. However, to estimate the continuum intensity below 15 keV, the L-line intensity must first be estimated and subtracted. Because of this procedure, there is also a large uncertainty in the continuum intensity

below 15 keV for the two units with beryllium windows. For example, both the 60-kV Picker and the 275-kV Triplett-Barton units show a peak in the continuum below 10 keV, but it is not clear whether these peaks are real. They appeared after the L-line removal and the filtration corrections were made. They may represent tungsten L-edge structure in the continuum which was not clearly resolved because of the superimposed L lines.

The K-edge jump ratios are plotted in Fig. 34 as a function of tube potential. The ratio increases linearly with potential above 80 kV, but appears to be leveling off above 200 kV.

c. Integrated Photon and Energy Flux

The total number of continuum photons emitted by the target was obtained by integrating the curves in Figs. 30 to 33, and the results are given in Table V. The L- and K-line intensities given in Figs. 10, 15, 20, and 25 were corrected for attenuation, converted to target intensities, and totalled. The L- and K-line photon totals are given in Table V. The L-line intensity of the 100-kV Picker and 300-kV Norelco spectra could not be determined, because of the large inherent filtration.

The photon spectra were converted to energy in units of ergs/sec-mA-sr, and the totals for both the continuum and lines are given in Table V. The total continuum energy flux is plotted in Fig. 35, and the total L- and K-line energy flux in Fig. 36, as a function of tube potential for the four x-ray units. The 100-kV Picker, 275-kV Triplett-Barton, and 300-kV Norelco continuum and K-line totals appear to be following a similar trend. However, the 60-kV Picker continuum and L-line totals lie a factor of 2 to 3 above the others. This may be due in part to the 45° target angle of the 60-kV Picker unit, compared to the 20 to 22° target angle of the other units. Photons produced in the tungsten target are attenuated by a thickness $x/\tan\theta$ as they leave the target, where x is the target thickness traversed by the electron before photon emission. Consequently, the 60-kV Picker photons suffer less attenuation than the photons from the other units. In addition, one would expect the 60-kV Picker and 300-kV Norelco constant-potential units to have greater intensity than the other two units which are self-rectified.

Table V gives the ratio of the L- and K-line photon fluxes to the total photon flux. The ratio of the line to total energy flux is also given in Table V and plotted in Fig. 37 as a function of tube potential. The L-to-total ratio, which is zero below the L edges (10 to 12 keV), builds up to a value of 0.32 at 20 keV, and then decreases steadily as the tube potential increases. The K-to-total ratio also builds up rapidly above the K edge (69.5 keV) as the tube potential increases, and then levels off around 150 kV.

d. X-Ray Production Efficiency

The efficiency for x-ray production, ε, was defined by Compton and Allison[30] as

$$\varepsilon = \frac{\text{x-ray energy}}{\text{cathode ray energy}} = kZV,$$

where z is the atomic number of the target, V the tube potential, and k a constant of proportionality in units of reciprocal volts. Using measurements made before 1935, Compton and Allison concluded that k was approximately 1.1×10^{-6} $(kV)^{-1}$. After studying later measurements and calculations, Evans[31] in 1955 concluded that a better value for k was 0.7×10^{-6} $(kV)^{-1}$. From the L, K, and continuum intensities given in Table V, one can obtain the total x-ray energy, and thus the efficiency and proportionality constant. The x-ray production efficiency and k are plotted as a function of tube potential in Figs. 38 and 39, respectively. The value of k varies between 0.22 and 0.74×10^{-1} $(kV)^{-1}$. The values of k obtained with the constant-potential units tend to increase as the tube potential increases.

TABLE V

TOTAL PHOTON AND ENERGY FLUX

X-Ray Unit	Potential (kV)	C	L	L/(L+C)	K	K/(K+C)
		Photons/sec-mA-sr, $\times 10^{-12}$				
300-kV Norelco	100	2.09			0.124	0.0560
	150	4.89			0.625	0.113
	200	8.20			1.37	0.144
	250	13.1			2.22	0.145
	300	18.1			3.23	0.151
275-kV Triplett-Barton	60	1.87	0.907	0.327		
	80	2.82	1.16	0.292	0.017	0.0060
	100	4.09	1.38	0.253	0.098	0.0234
	150	6.73	1.77	0.208	0.454	0.0632
	200	9.07	1.90	0.173	0.778	0.0790
100-kV Picker	40	0.774				
	60	1.38				
	80	1.93			0.0134	0.0069
	100	2.67			0.0689	0.0252
60-kV Picker	12	0.231				
	20	0.668	0.299	0.309		
	40	2.28	1.33	0.368		
	60	3.92	2.34	0.373		
		Ergs/sec-mA-sr, $\times 10^{-5}$				
300-kV Norelco	100	1.68			0.120	0.067
	150	4.81			0.608	0.112
	200	9.39			1.33	0.124
	250	16.2			2.16	0.117
	300	24.7			3.13	0.112
275-kV Triplett-Barton	60	0.573	0.136	0.192		
	80	1.08	0.175	0.139	0.0165	0.0150
	100	1.92	0.208	0.0981	0.0947	0.0471
	150	4.34	0.266	0.0577	0.439	0.0920
	200	7.22	0.284	0.0379	0.754	0.0946
100-kV Picker	40	0.224				
	60	0.518				
	80	0.844			0.0129	0.0151
	100	1.36			0.0667	0.0468
60-kV Picker	12	0.0251				
	20	0.0947	0.0448	0.322		
	40	0.491	0.199	0.289		
	60	1.16	0.351	0.232		

C = Continuum
L = L lines
K = K lines

REFERENCES

1. H. Kulenkampff, Ann. Physik, 69, 548 (1922).

2. H. Kulenkampff and L. Schmidt, Ann. Physik, 43, 494 (1943).

3. R. Fuch and H. Kulenkampff, Z. Physik, 137, 583 (1955).

4. M. Ehrlich, J. Res. Natl. Bur. Std., 54, 107 (1955).

5. P. K. S. Wang, R. J. Raridon, and M. Tidwell, Brit. J. Radiol., 30, 70 (1957).

6. J. H. Aitken and W. R. Dixon, Natl. Res. Council Can. 4864 (1958).

7. G. Hettinger and N. Starfelt, Acta Radiol., 50, 381 (1958).

8. N. A. Dyson, Proc. Phys. Soc., 73, 924 (1959).

9. D. V. Cormack and D. G. Burke, Radiology, 74, 743 (1960).

10. L. D. Skarsgard and H. E. Johns, Rad. Res., 14, 231 (1961).

11. E. R. Epp and H. Weiss, Phys. Med. Biol., 11, 225, (1966).

12. L. H. J. Peaple and A. K. Burt, Phys. Med. Biol., 14, 73 (1969).

13. E. Casnati, M. P. Fioratti, and S. Piermattei, Comitato Nazionale per l'E-Nergia Nucleare, Rome (Italy), RT/PROT (69) 16, 1968.

14. M. H. Unsworth and J. R. Greening, Phys. Med. Biol., 15, 621, 631 (1970).

15. H. W. Koch and J. W. Motz, Rev. Mod. Phys., 31, 920 (1959).

16. S. T. Stephenson, Handbuch der Physik, 30, 337 (1957).

17. Natl. Bur. Std. Handbook 78, 41 (1961).

18. ICRU Report 17, 8 (1970).

19. G. Drexler and M. Gossrau, Institut für Strahlenschutz, Neuherberg bei Munchen Report GSF-Bericht S45, 1968.

20. R. C. Placious, J. Appl. Phys., 38, 2030 (1967).

21. D. H. Rester, W. E. Dance, and J. H. Derrickson, J. Appl. Phys., 41, 2682 (1970).

22. H. I. Israel, D. W. Lier, and E. Storm, Nucl. Instr. Methods, 91, 141 (1971).

23. H. A. Kramers, Phil Mag., 46, 836 (1923).

24. G. Wentzel, Z. Physik, 27, 257 (1924).

25. A. Sommerfeld, Ann. Physik, 11, 257 (1931).

26. P. Kirkpatrick and L. Wiedmann, Phys. Rev., 67, 321 (1945).

27. M. J. Berger and S. M. Seltzer, Natl. Bur. Std. Rpts. 9836 and 9837, 1968.

28. R. C. Emigh, Los Alamos Scientific Laboratory Report LA-4097-MS, 1970.

29. E. Storm and H. I. Israel, Nuclear Data Tables, A7, 565 (1970).

30. A. H. Compton and S. K. Allison, X-Rays in Theory and Experiment, D. Van Nostrand Co., New York, p. 89 (1935).

31. R. D. Evans, The Atomic Nucleus, McGraw-Hill, New York, p. 616 (1955).

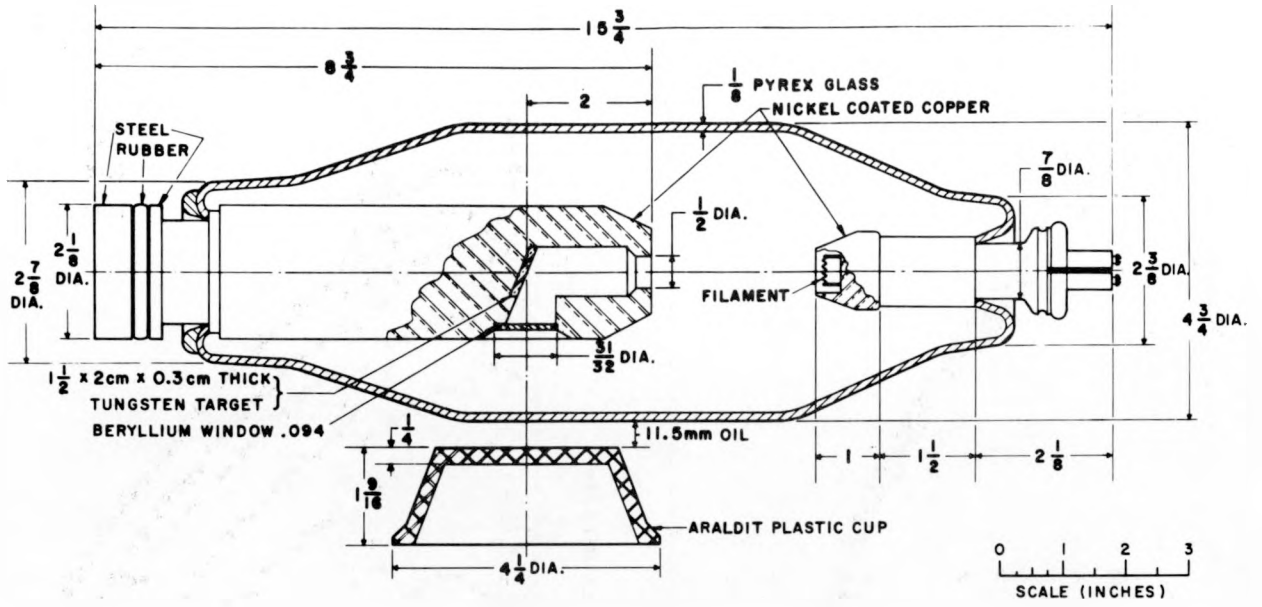

NORELCO 300kV — 10mA X-RAY TUBE

Fig. 1. Sketch of the 300-kV Norelco x-ray tube showing the inherent filtration.

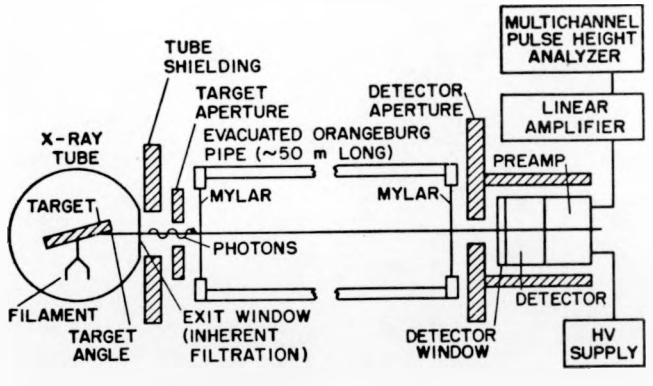

Fig. 2. Schematic diagram showing the experimental arrangement for the measurement of x-ray spectra.

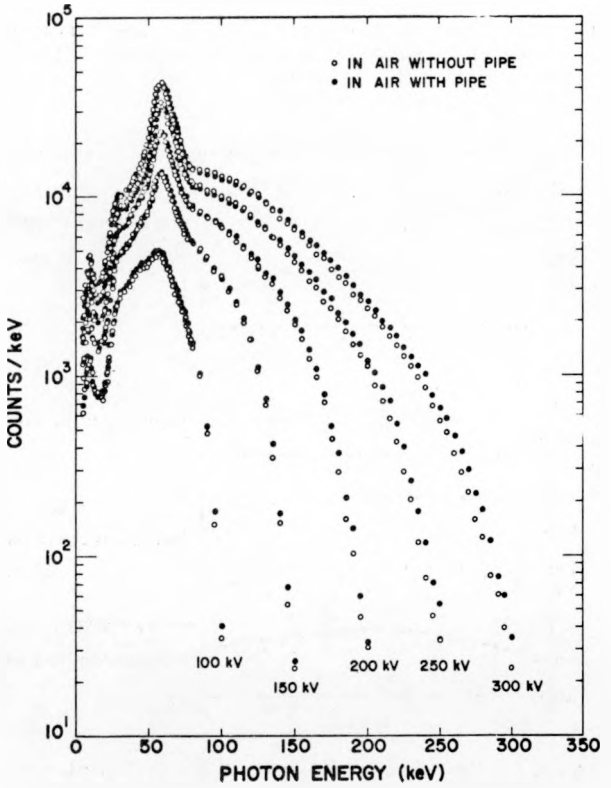

Fig. 3. Spectral measurements in air with and without the Orangeburg pipe.

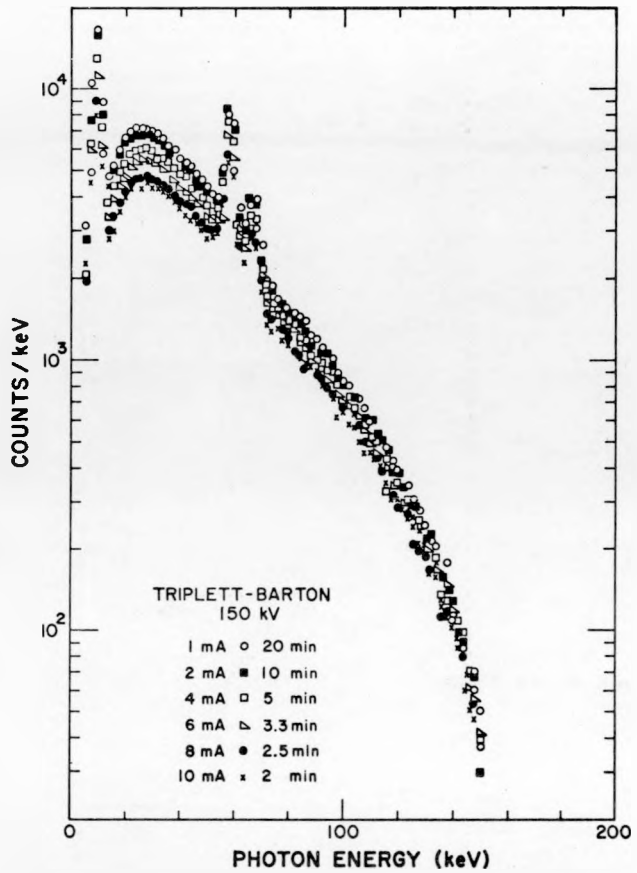

Fig. 4. Triplett-Barton 150-kV spectrum at different tube currents measured with the germanium detector.

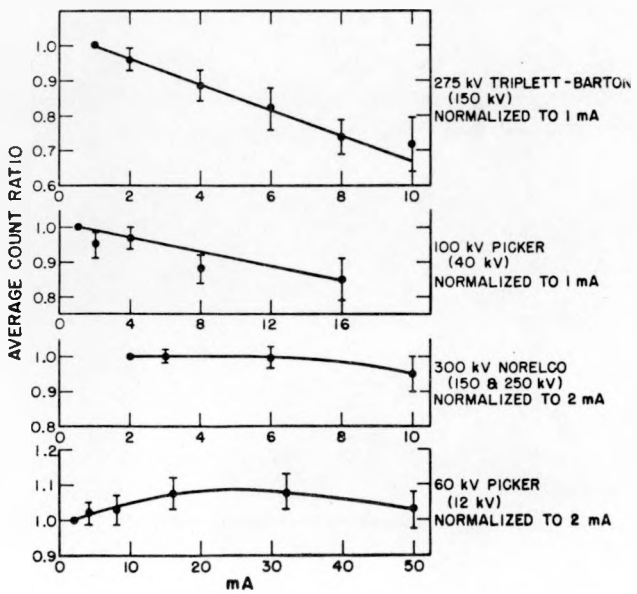

Fig. 5. Variation in count as a function of tube current for all four x-ray units. Tube potentials in parenthesis are those at which measurements were made.

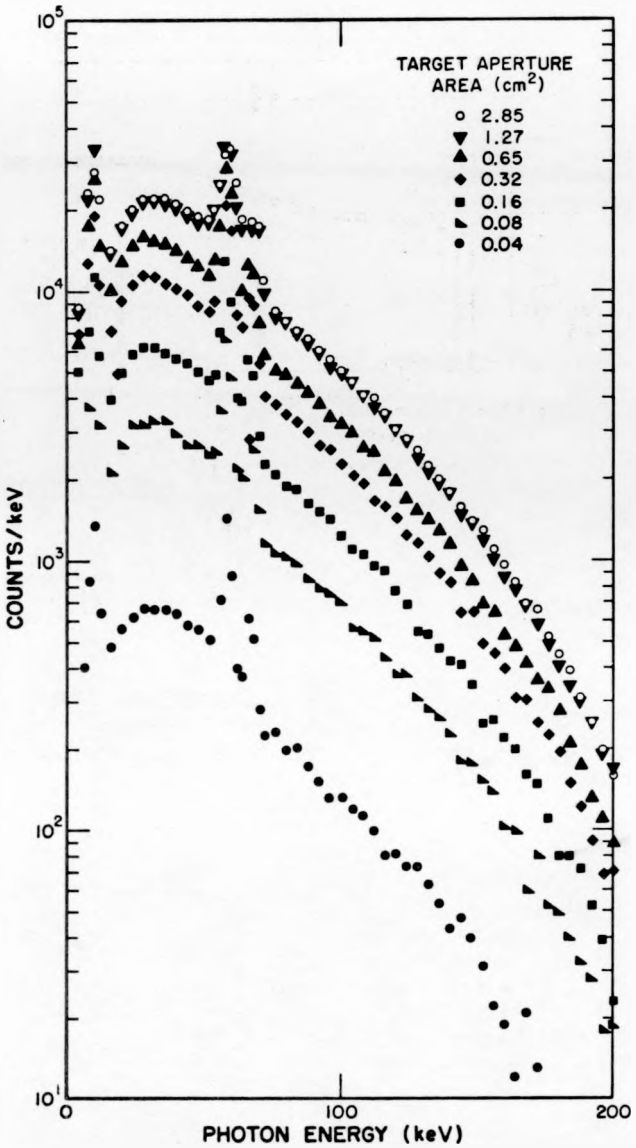

Fig. 6. Triplett-Barton 200-kV spectrum measured with the germanium detector and various target apertures.

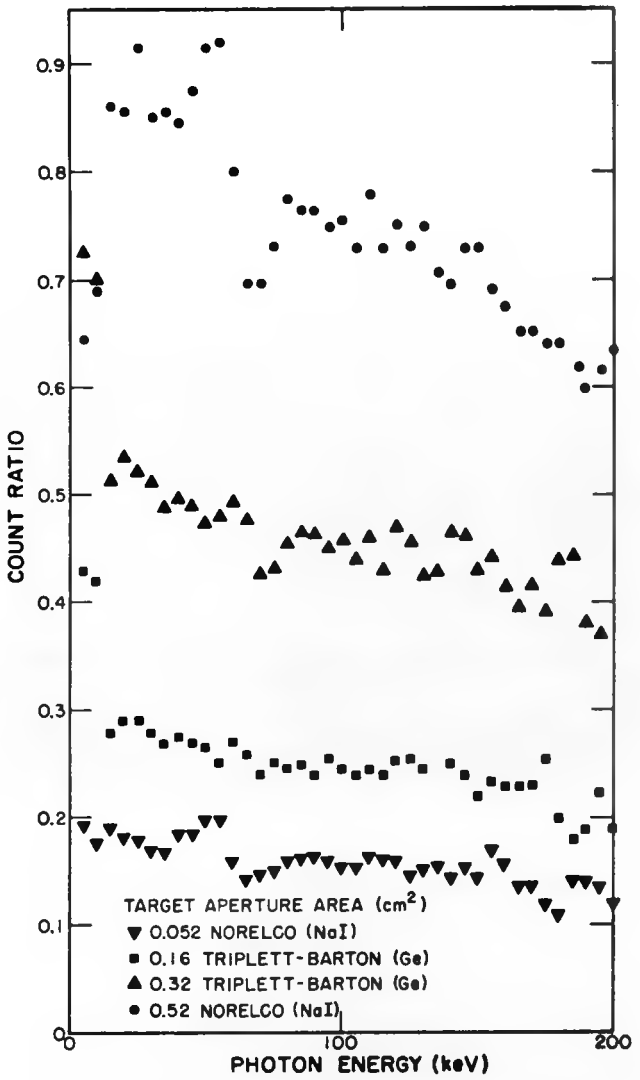

Fig. 7. Variation in count as a function of photon energy for four different target apertures.

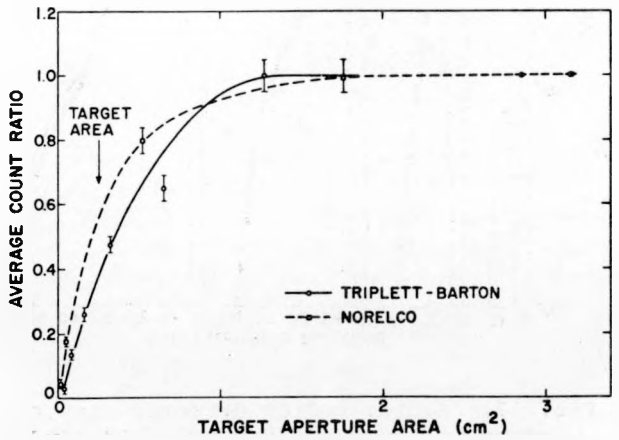

Fig. 8. Variation in count as a function of target aperture area.

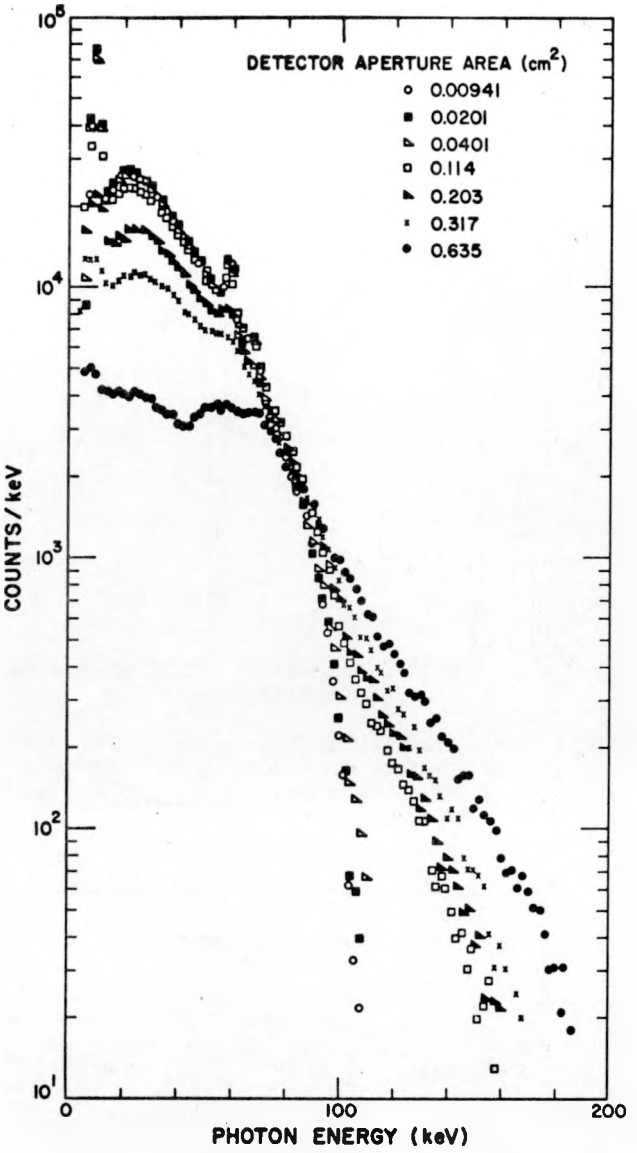

Fig. 9. Triplett-Barton 100-kV spectrum measured with the germanium detector at various detector apertures.

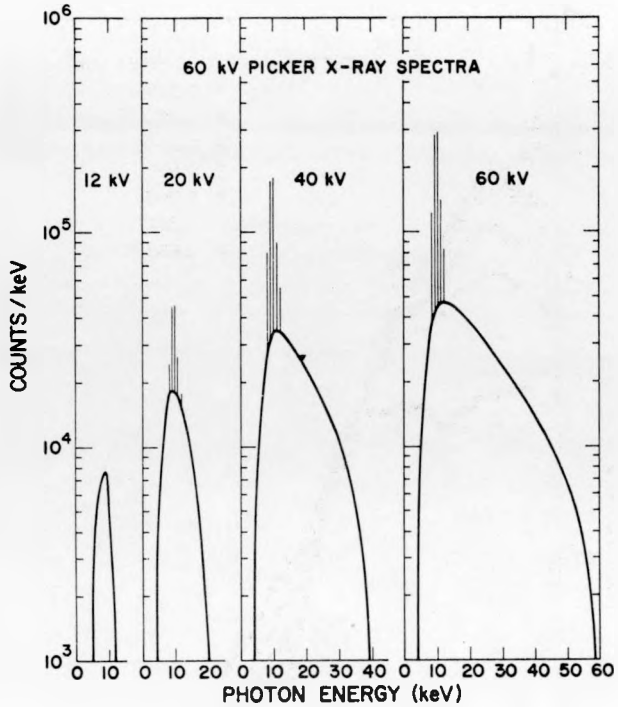

Fig. 10. Undistorted 12-, 20-, 40-, and 60-kV spectra from the 60-kV Picker x-ray unit. Experimental conditions are given in Table IV.

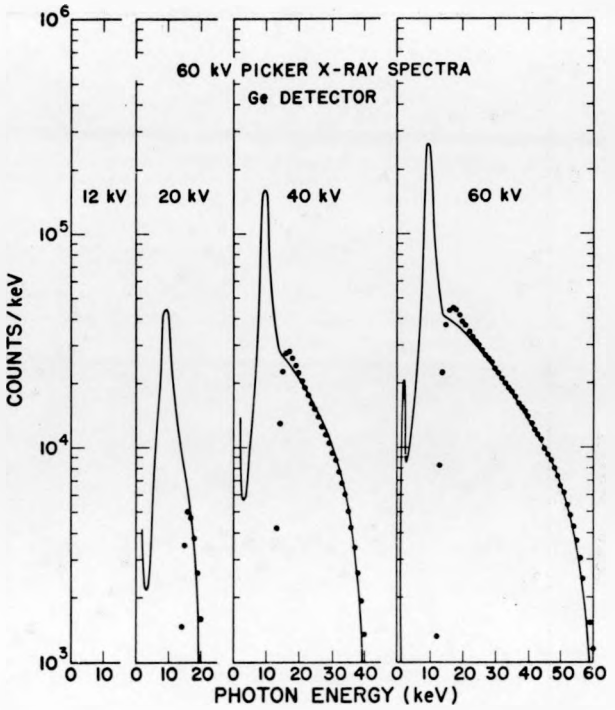

Fig. 12. Germanium detector measurements of the 60-kV Picker x-ray spectra. Points are measured values and solid lines are Monte Carlo calculations.

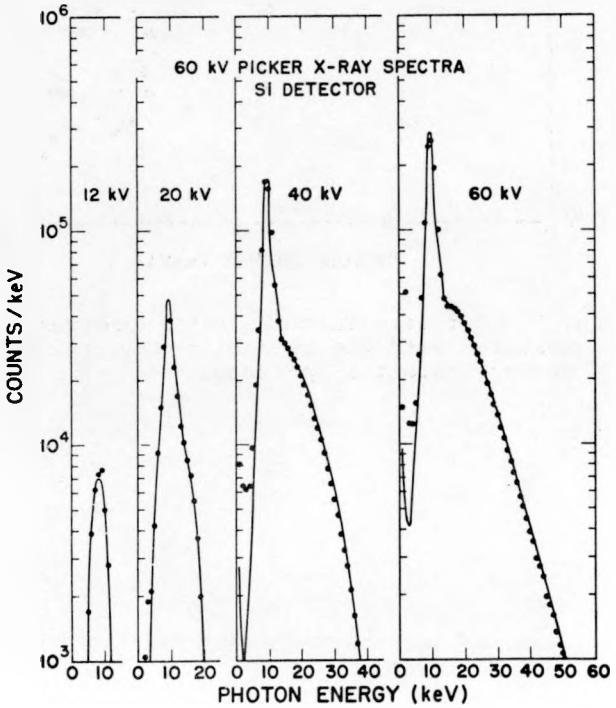

Fig. 11. Silicon detector measurements of the 60-kV Picker x-ray spectra. Points are measured values, and solid lines are Monte Carlo calculations

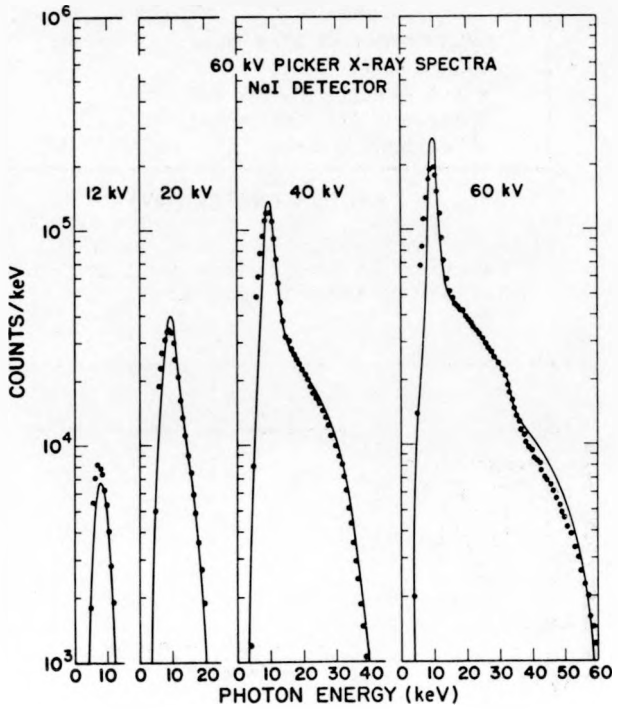

Fig. 13. Sodium iodide detector measurements of the 60-kV Picker x-ray spectra. Points are measured values, and solid lines are Monte Carlo calculations.

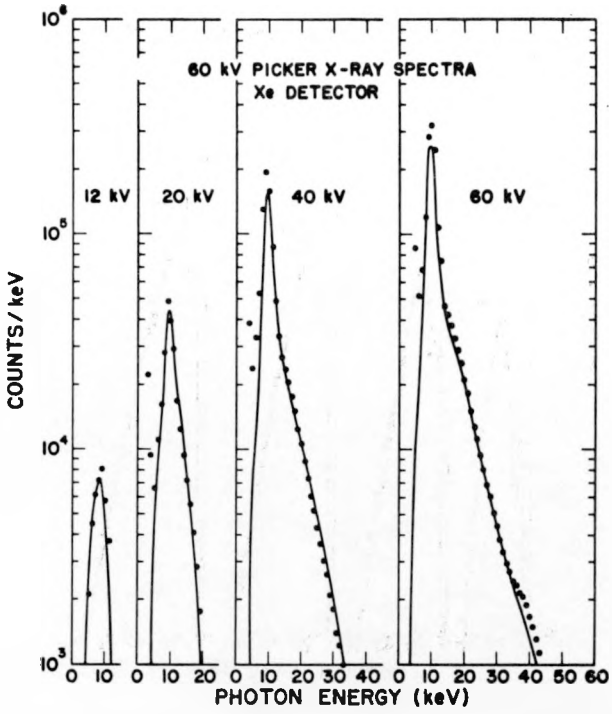

Fig. 14. Xenon detector measurements of the 60-kV Picker x-ray spectra. Points are measured values, and solid lines are Monte Carlo calculations.

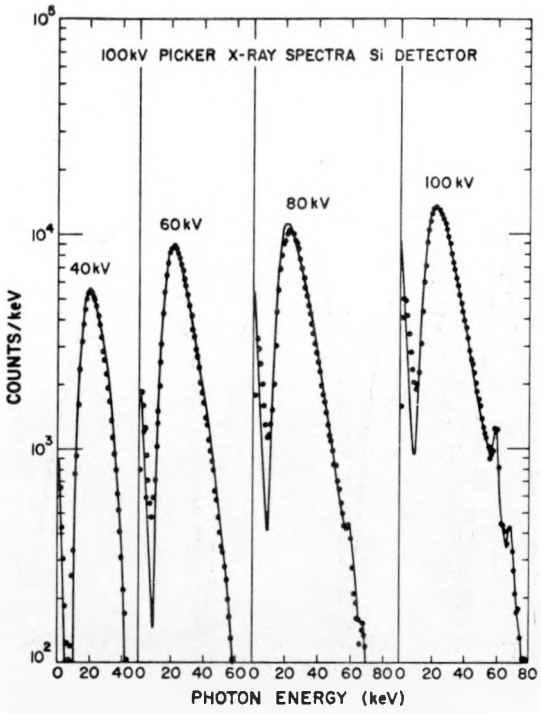

Fig. 16. Silicon detector measurements of the 100-kV Picker x-ray spectra. Points are measured values, and solid lines are Monte Carlo calculations.

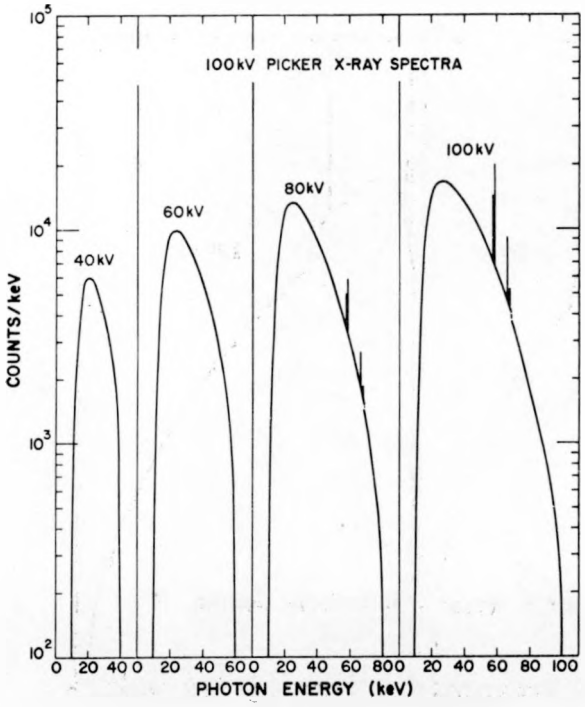

Fig. 15. Undistorted 40-, 60-, 80-, and 100-kV spectra from the 100-kV Picker x-ray unit. Experimental conditions are given in Table IV.

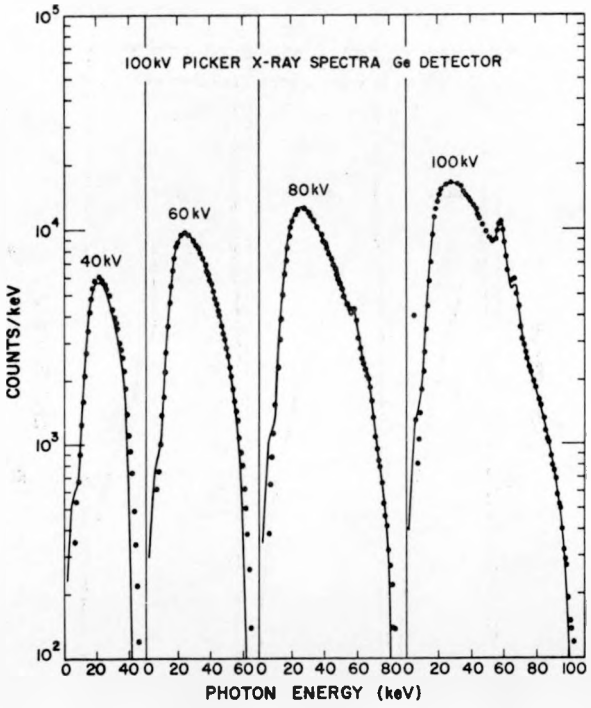

Fig. 17. Germanium detector measurements of the 100-kV Picker x-ray spectra. Points are measured values, and solid lines are Monte Carlo calculations.

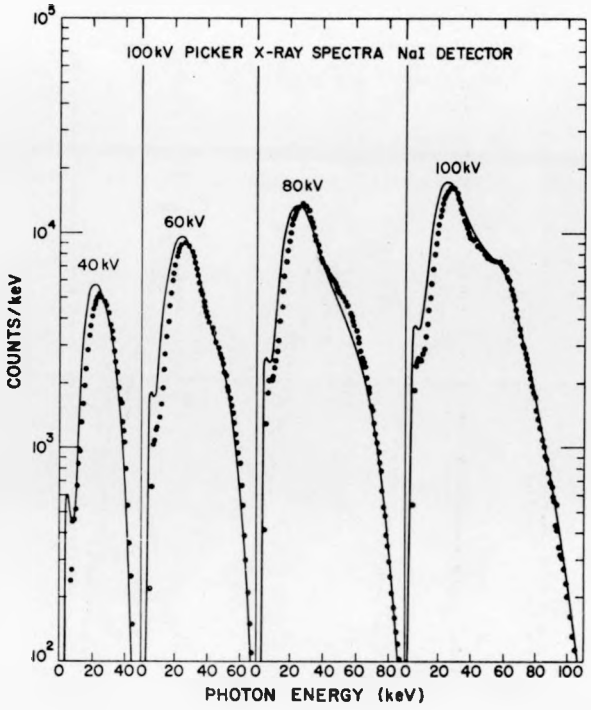

Fig. 18. Sodium iodide detector measurements of the 100-kV Picker x-ray spectra. Points are measured values, and solid lines are Monte Carlo calculations.

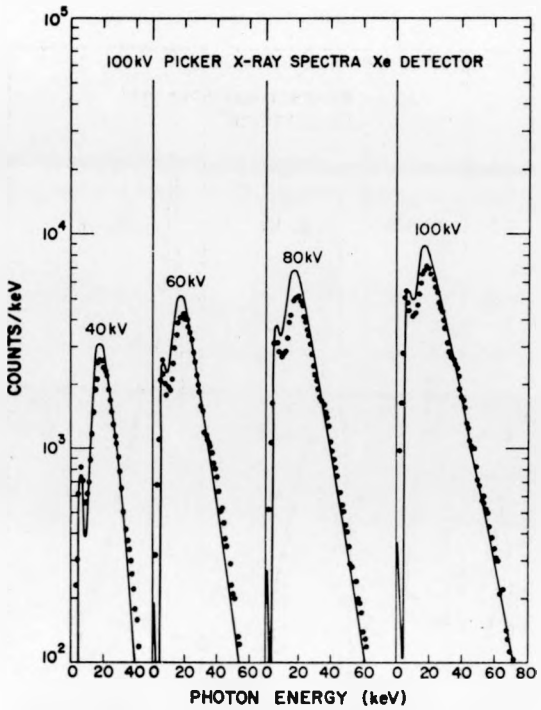

Fig. 19. Xenon detector measurements of the 100-kV Picker x-ray spectra. Points are measured values, and solid lines are Monte Carlo calculations.

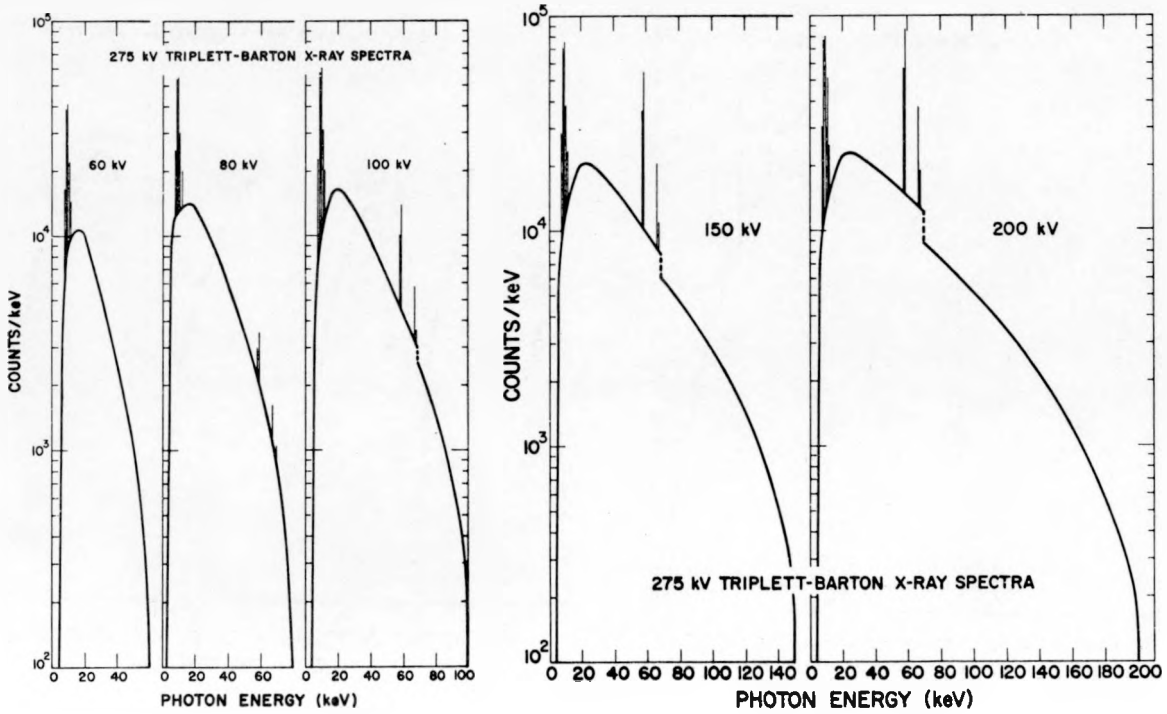

Fig. 20. Undistorted spectra from the 275-kV Triplett-Barton x-ray unit. Experimental conditions are given in Table IV.

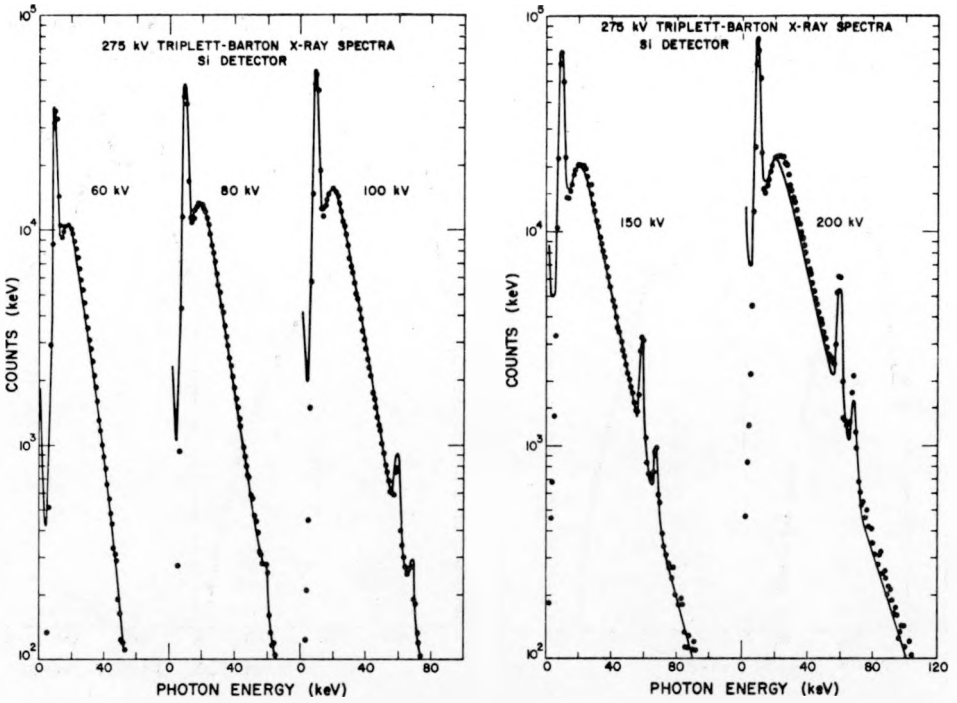

Fig. 21. Silicon detector measurements of the 275-kV Triplett-Barton x-ray spectra. Points are measured values, and solid lines are Monte Carlo calculations.

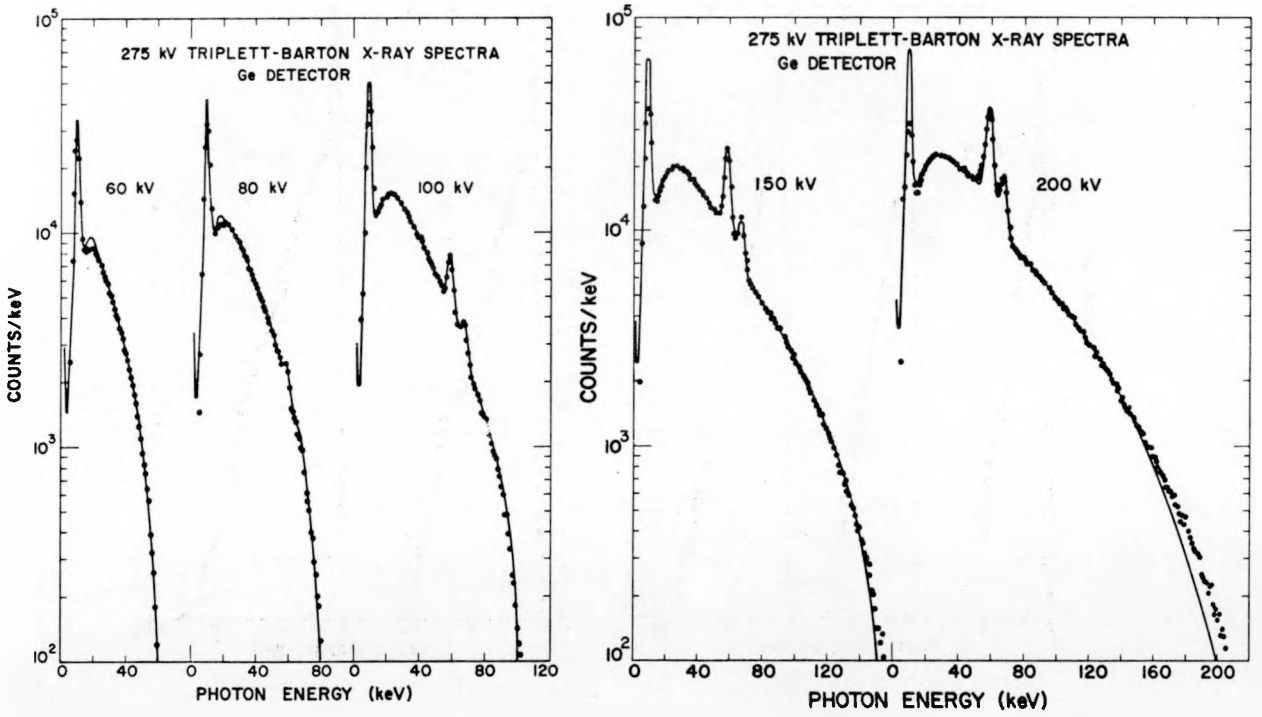

Fig. 22. Germanium detector measurements of the 275-kV Triplett-Barton x-ray spectra. Points are measured values, and solid lines are Monte Carlo calculations.

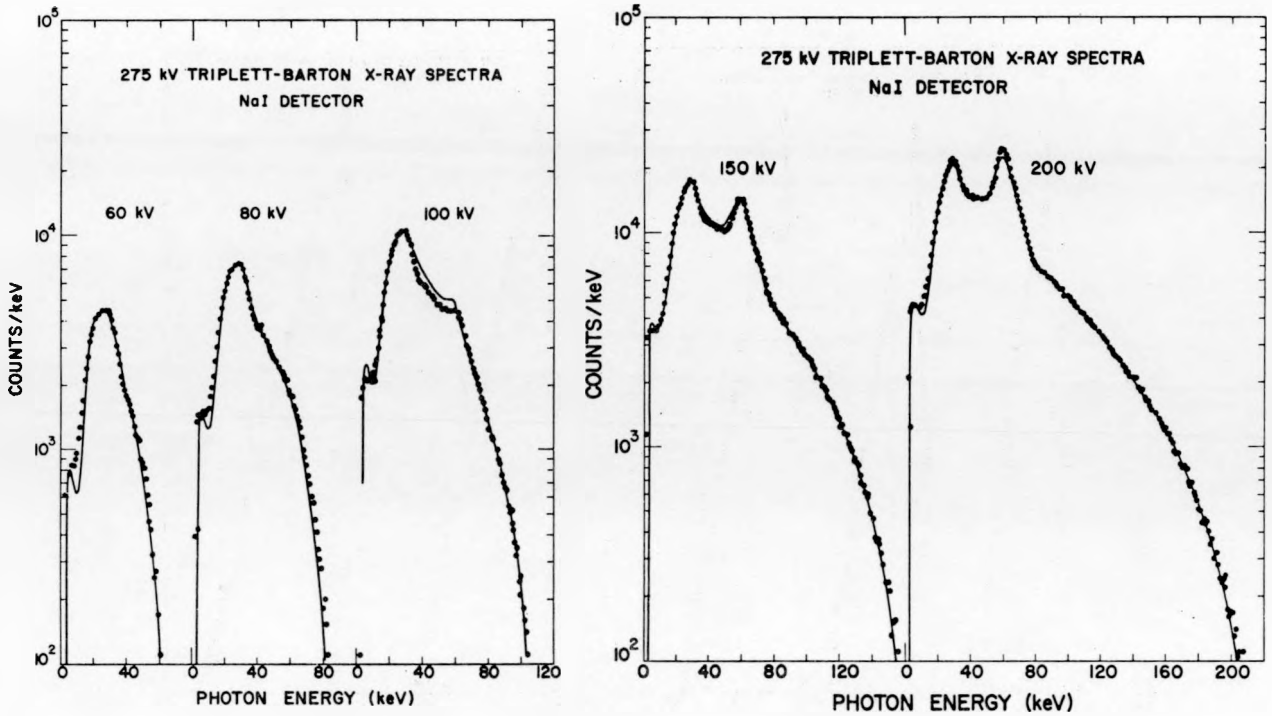

Fig. 23. Sodium iodide detector measurements of the 275-kV Triplett-Barton x-ray spectra. Points are measured values, and solid lines are Monte Carlo calculations.

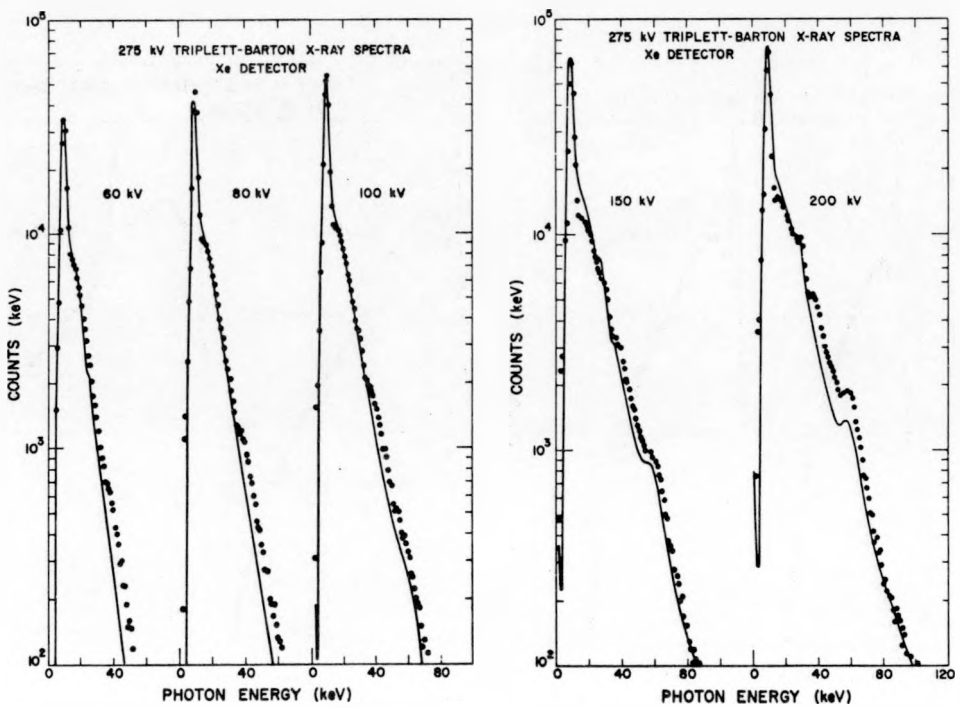

Fig. 24. Xenon detector measurements of the 275-kV Triplett-Barton x-ray spectra. Points are measured values, and solid lines are Monte Carlo calculations.

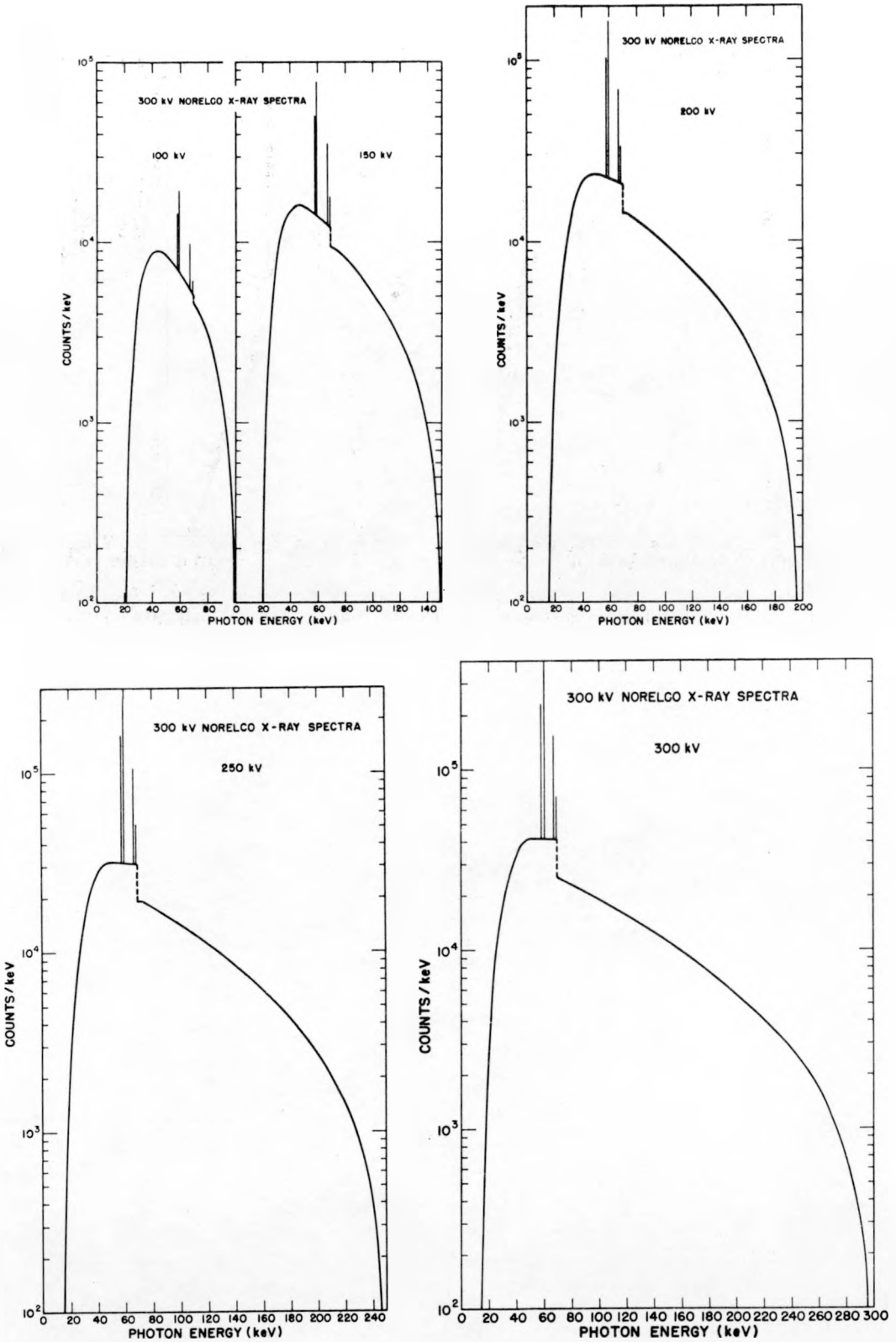

Fig. 25. Undistorted spectra from the 300-kV Norelco x-ray unit. Experimental conditions are given in Table IV.

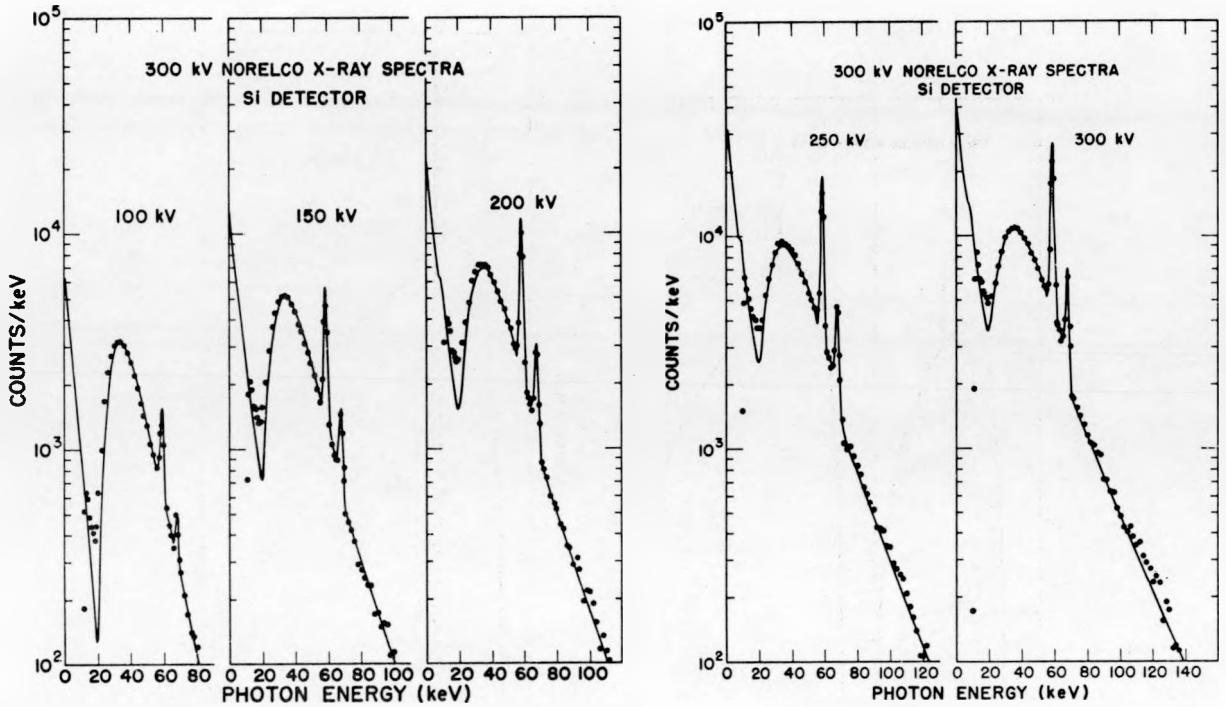

Fig. 26. Silicon detector measurements of the 300-kV Norelco x-ray spectra. Points are measured values, and solid lines are Monte Carlo calculations.

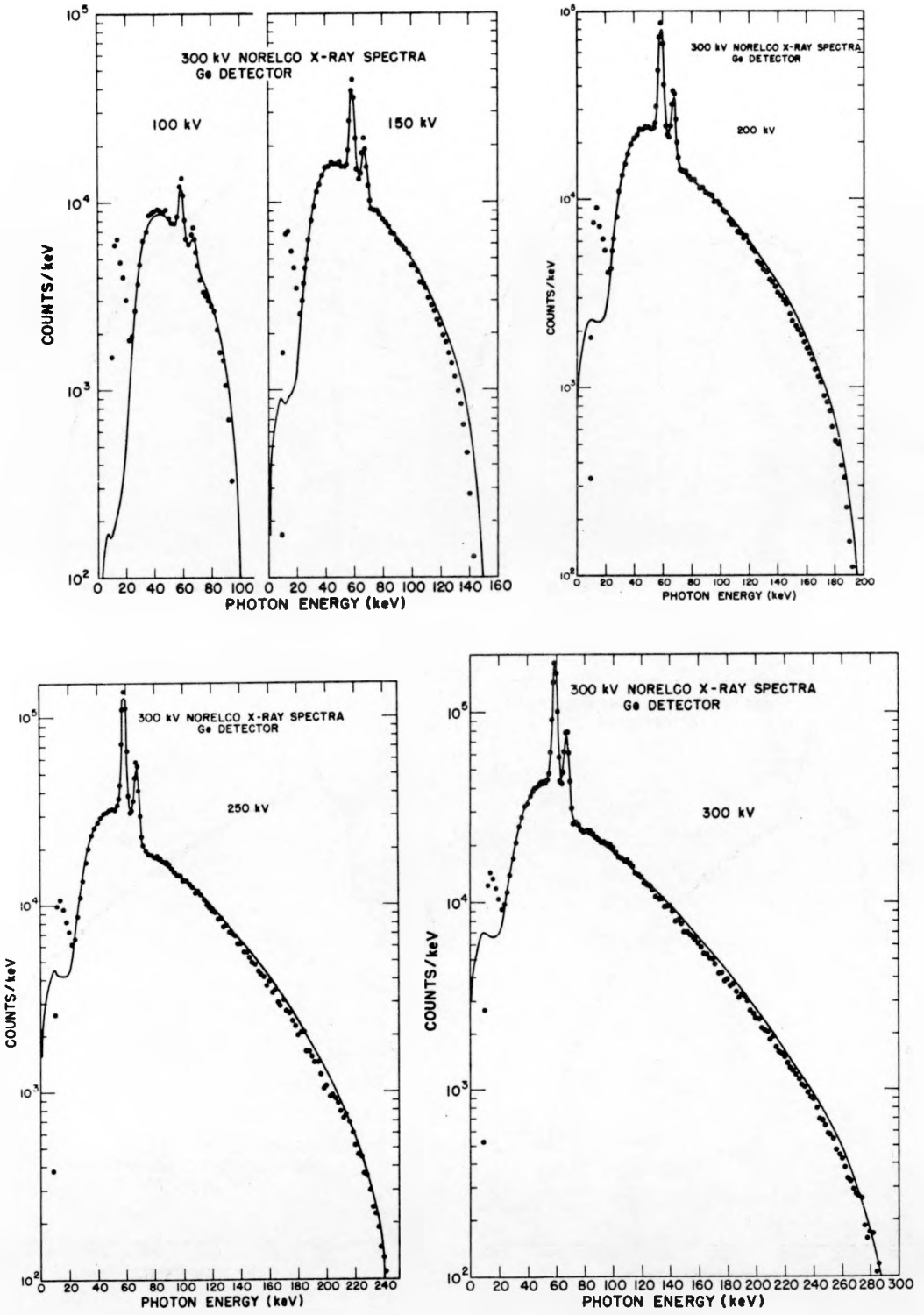

Fig. 27. Germanium detector measurements of the 300-kV Norelco x-ray spectra. Points are measured values, and solid lines are Monte Carlo calculations.

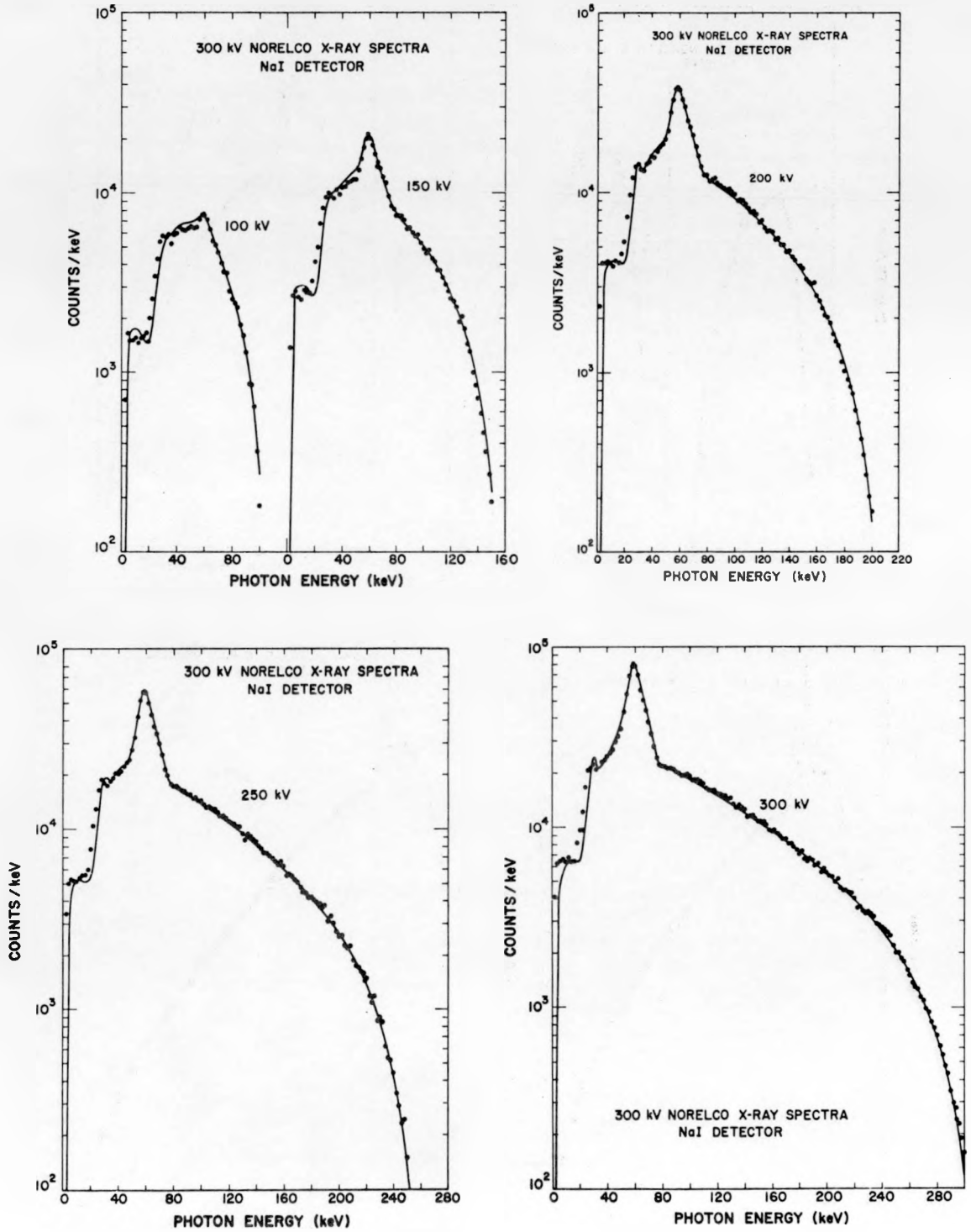

Fig. 28. Sodium iodide detector measurements of the 300-kV Norelco x-ray spectra. Points are measured values, and solid lines are Monte Carlo calculations.

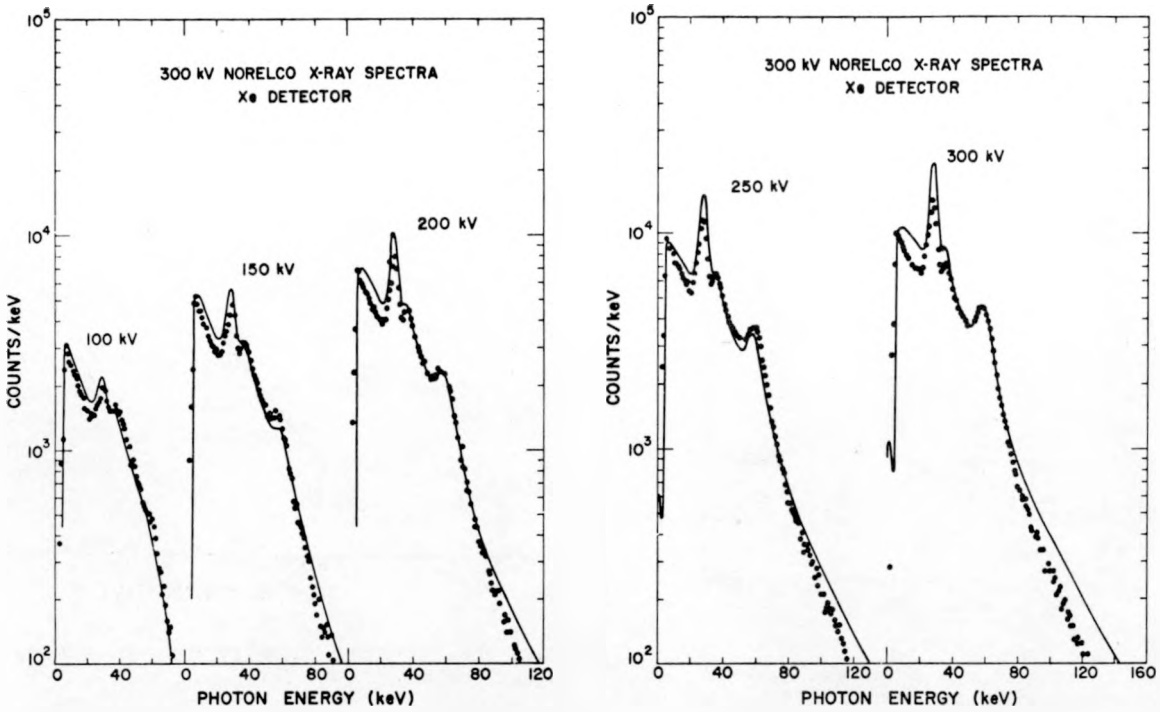

Fig. 29. Xenon detector measurements of the 300-kV Norelco x-ray spectra. Points are measured values, and solid lines are Monte Carlo calculations.

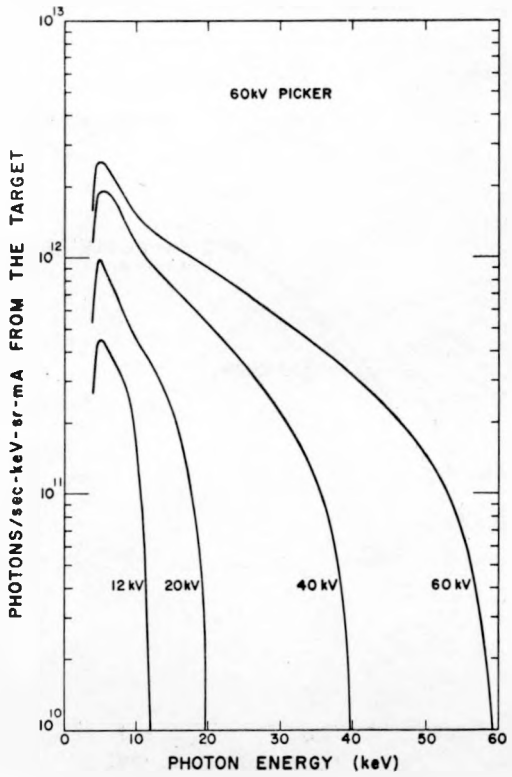

Fig. 30. Photon flux from the 60-kV Picker target as a function of photon energy. Characteristic lines have been omitted.

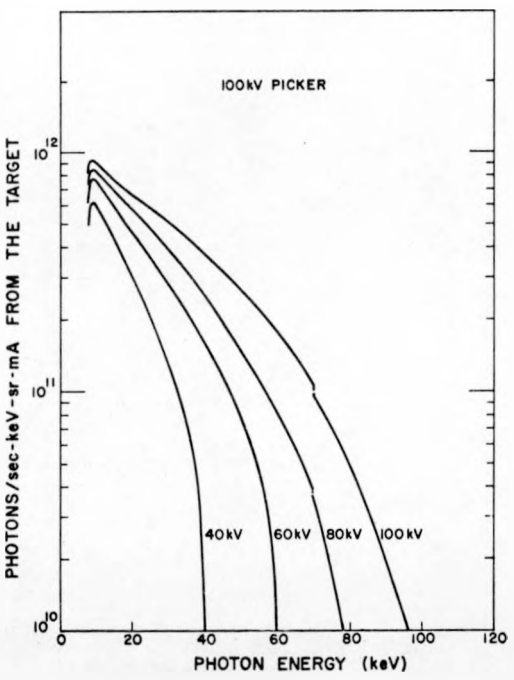

Fig. 31. Photon flux from the 100-kV Picker target as a function of photon energy. Characteristic lines have been omitted.

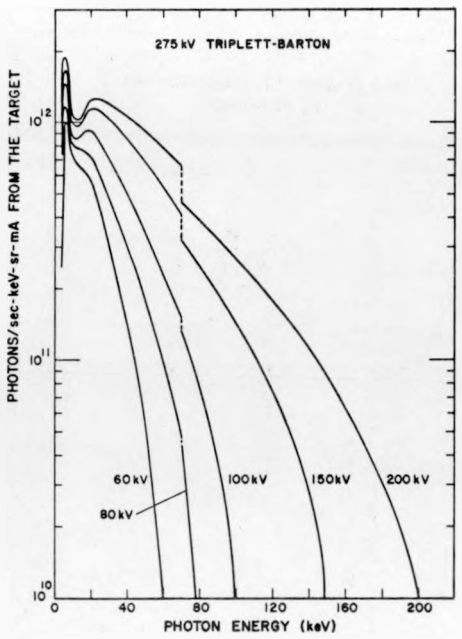

Fig. 32. Photon flux from the 275-kV Triplett-Barton target as a function of photon energy. Characteristic lines have been omitted.

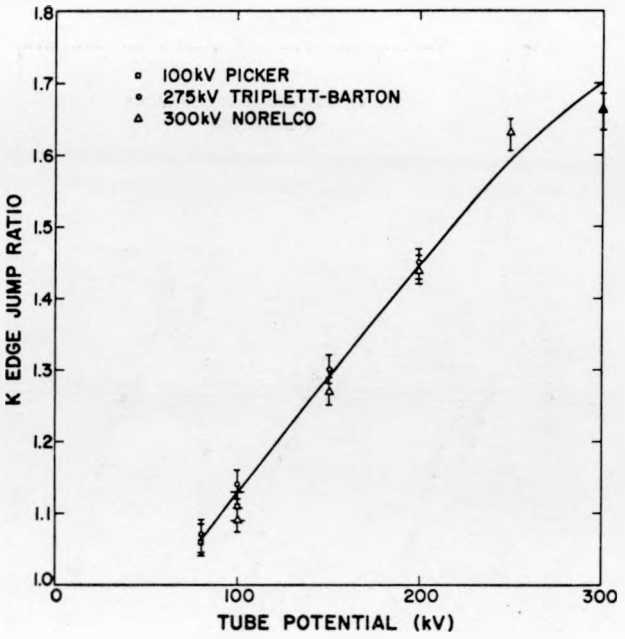

Fig. 34. K-edge jump ratios as a function of tube potential.

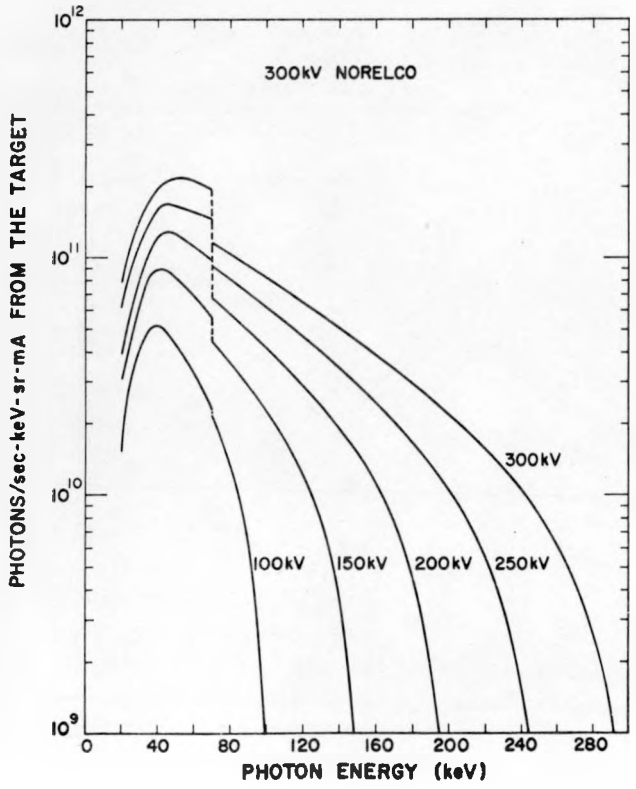

Fig. 33. Photon flux from the 300-kV Norelco target as a function of photon energy. Characteristic lines have been omitted.

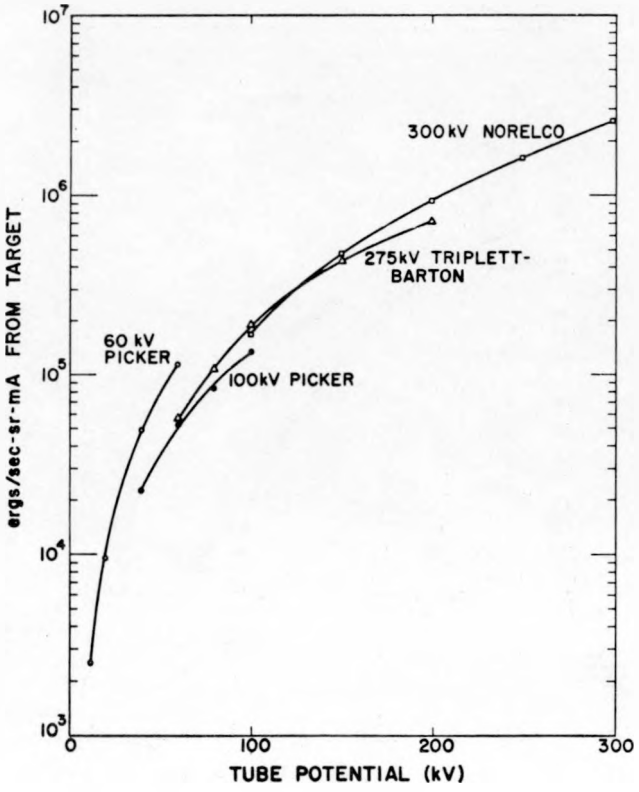

Fig. 35. Total continuum energy flux emitted from the target as a function of excitation potential.

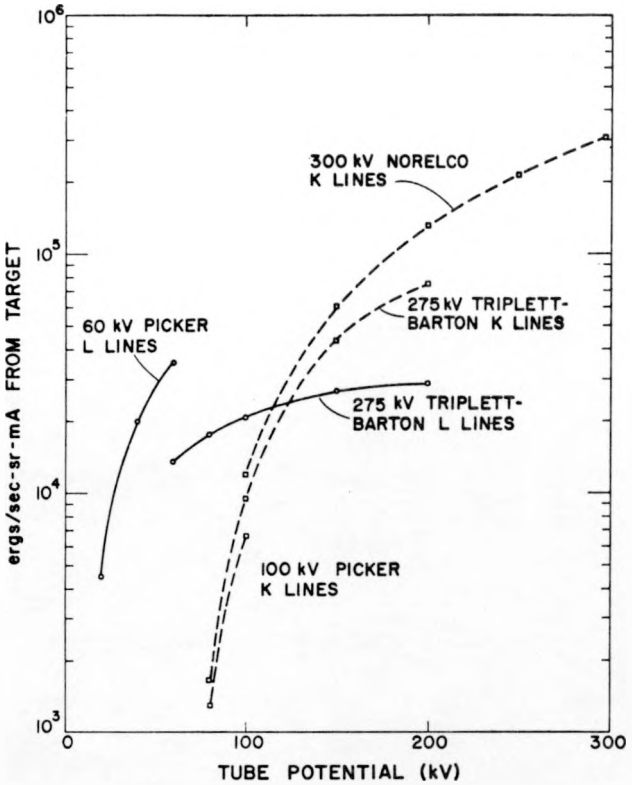

Fig. 36. Total L- and K-line energy flux emitted from the target as a function of excitation potential.

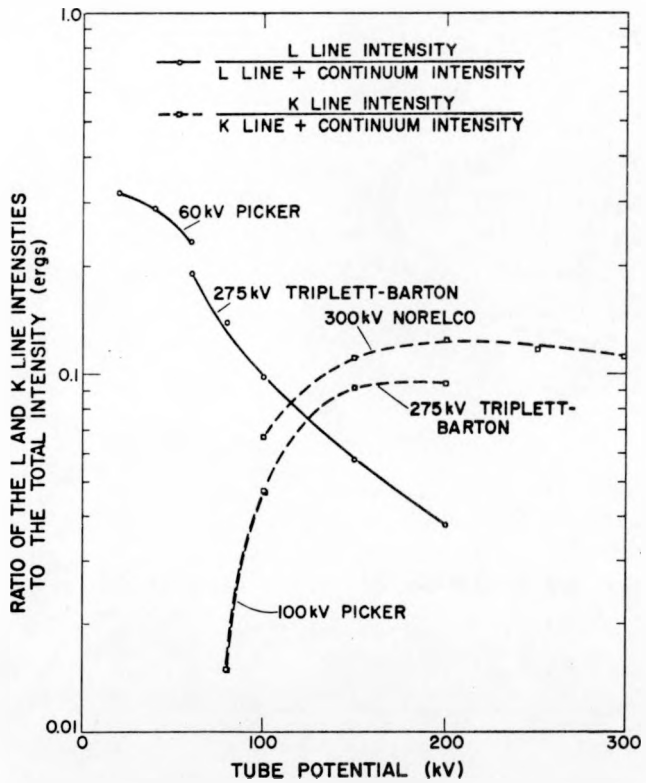

Fig. 37. Ratio of the L- and K-line energy flux to the total energy flux as a function of excitation potential.

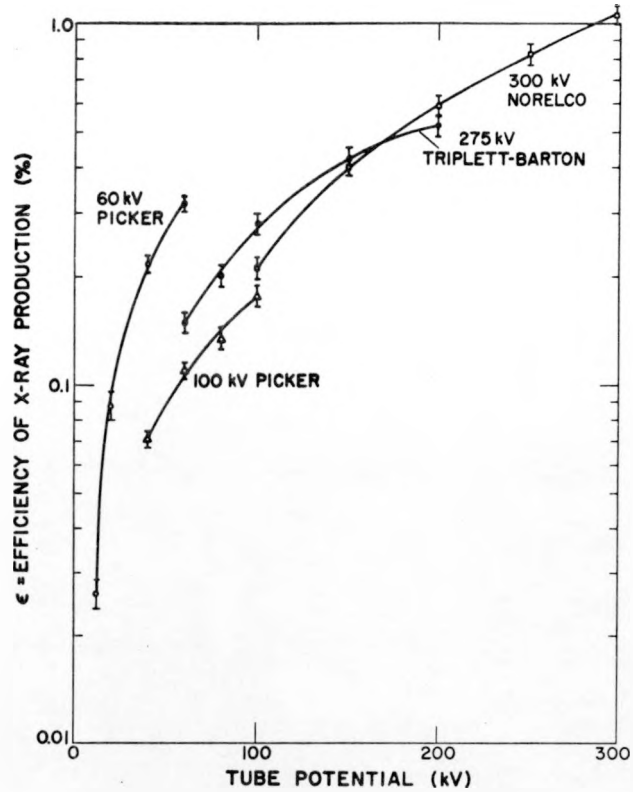

Fig. 38. X-ray production efficiency as a function of tube potential.

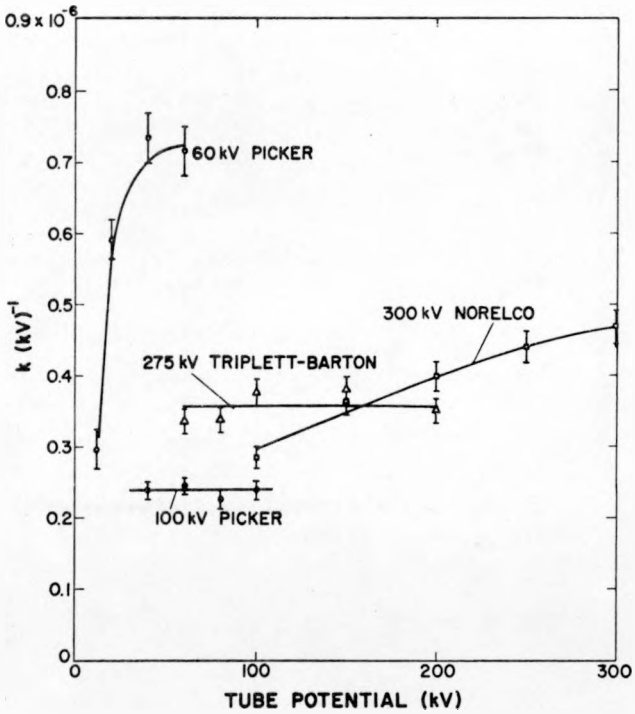

Fig. 39. The constant of proportionality, k, as a function of tube potential.